ELSEVIER

An overview of the development of the first wall and other principal components of a laser fusion power plant

John D. Sethian [a,*], A. Rene Raffray [b], Jeffery Latkowski [c], James P. Blanchard [d], Lance Snead [e], Timothy J. Renk [f], Shahram Sharafat [g]

[a] *Plasma Physics Division, Naval Research Laboratory, 4555 Overlook Av. SW, Washington, DC 20375, United States*
[b] *University of California, San Diego, La Jolla, CA 92093, United States*
[c] *Lawrence Livermore National Laboratory, Livermore, CA 94550, United States*
[d] *University of Wisconsin, Madison, WI 53706, United States*
[e] *Oak Ridge National Laboratory, Oak Ridge, TN 37831, United States*
[f] *Sandia National Laboratory, Albuquerque, NM 87185, United States*
[g] *University of California, Los Angeles, Los Angeles, CA 90095, United States*

Abstract

This paper introduces the JNM Special Issue on the development of a first wall for the reaction chamber in a laser fusion power plant. In this approach to fusion energy a spherical target is injected into a large chamber and heated to fusion burn by an array of lasers. The target emissions are absorbed by the wall and encapsulating blanket, and the resulting heat converted into electricity. The bulk of the energy deposited in the first wall is in the form of X-rays (1.0–100 keV) and ions (0.1–4 MeV). In order to have a practical power plant, the first wall must be resistant to these emissions and suffer virtually no erosion on each shot. A wall candidate based on tungsten armor bonded to a low activation ferritic steel substrate has been chosen as the initial system to be studied. The choice was based on the vast experience with these materials in a nuclear environment and the ability to address most of the key remaining issues with existing facilities. This overview paper is divided into three parts. The first part summarizes the current state of the development of laser fusion energy. The second part introduces the tungsten armored ferritic steel concept, the three critical development issues (thermo-mechanical fatigue, helium retention, and bonding) and the research to address them. Based on progress to date the latter two appear to be resolvable, but the former remains a challenge. Complete details are presented in the companion papers in this JNM Special Issue. The third part discusses other factors that must be considered in the design of the first wall, including compatibility with blanket concepts, radiological concerns, and structural considerations.
Published by Elsevier B.V.

1. Introduction

A major program is underway to develop the science and technology for a practical fusion energy source based on lasers, direct drive targets, and solid wall chambers [1]. This concept is shown schematically in Fig. 1. A spherical pellet, five mm diameter

---

* Corresponding author. Tel.: +1 2027672705; fax: +1 2027670046.
 E-mail address: sethian@this.nrl.navy.mil (J.D. Sethian).
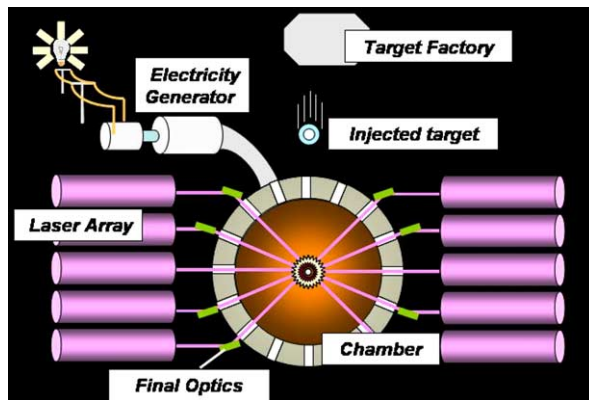
Fig. 1. Concept of a laser fusion power plant.

and containing deuterium and tritium, is injected into a large (several meter radius) chamber. When the target reaches the chamber center, it is directly illuminated with an array of intense laser beams with a total energy of around 2.5–3 MJ. The lasers ablate the outer part of the target. The ablated material is driven outward and, because of the rocket effect, the remaining inner part of the target (the 'fuel') is driven inward. When the fuel density reaches approximately forty times solid a hot spot is created in the central core. This region is hot enough to initiate or 'ignite' a DT fusion reaction. A fusion burn wave propagates radially outward. When the process is complete, approximately 30% of the DT fuel is expected to be burned. The energy from the target is released as neutrons and alpha (He^4) particles from the fusion reaction, along with X-rays and fast ions that are produced as the burn products propagate outward through the unburnt fuel. The X-rays and ions are entirely absorbed by the first wall of the chamber, and thus represent the major short term threat to the wall. Absorption of the neutrons also poses a threat, but this is a longer term phenomena which can be alleviated by periodic replacement of the first wall. Immediately behind the first wall is the 'blanket'. The blanket serves four functions: it stops the neutrons, it contains lithium to breed tritium for a subsequent implosion, it serves as a coolant to remove the heat deposited in both the first wall and blanket, and it transports the heat to an electricity generator. In a power plant this process would be repeated five times per second. Thus the chamber must return to a sufficiently quiescent state within 200 ms to allow high fidelity propagation of the lasers and injection of the target.

This approach has several inherent engineering advantages that reduce both the cost and risk of development. The system has a separable architecture and the components are modular. The complicated components – the lasers and the target factory – are physically isolated from the harsh environment of the reaction chamber. All the principal components can be developed separately before being integrated into the system, and just as importantly, the components can be independently upgraded as new technologies are developed. The first wall can be made in individual sectors that can be replaced during the plant lifetime. An example of how this can be accomplished was developed in the Sombrero Power Plant study [2]. The targets are spherical shells which can be mass produced in a droplet generator. There is also no target debris to recycle, other than of course the tritium. As the laser consists of an array of about 60 identical beam lines it is only necessary to develop and test one beam line in order to establish the viability of the technology. In addition to these potential advantages, significant advances have been made in developing the science and technology of the principal components. These factors make laser fusion an increasingly attractive path to a practical fusion energy source.

We propose to develop and demonstrate laser fusion energy in three phases. The present Phase I program is developing the critical science and technologies. Phase II will develop and integrate full size components. Phase III, will have three functions: (1) optimize laser–target and target–chamber interactions, (2) develop materials and components; and (3) generate net electricity fusion. We could be technically ready to start construction of Phase III within the next decade and start operations by 2020. This development could allow construction of pilot commercial plants well before 2050.

One of the key remaining challenges in Phase I is to develop a concept for a chamber first wall that can repetitively withstand the blast of X-rays, ions and neutrons from the target. Thermal and mechanical considerations require that the first wall be relatively thin, on the order of a few mm. As the system pulses at around 5 Hz, the first wall must suffer essentially no erosion ($\ll 1$ nm) on each shot in order to survive a full year of operation (1.5×10^8 pulses/year). Mass loss from the wall structure can occur through a number of processes, including: exfoliation, thermo-mechanical fatigue, radiation enhanced sublimation, physical sputtering, and chemical sputtering. Other deleterious effects can

be brought on by tritium retention and/or swelling. The relative severity of these depends on the choice of wall material.

To address these challenges and to make the problem tractable in a reasonable time frame (i.e. ready to field within the next 12–15 years), we have decided to concentrate on a 'front runner' first wall concept based on tungsten armored low activation ferritic steel. Other first wall systems considered were: (1) Tungsten armor on a Silicon Carbide (SiC) base, (2) a woven carbon/carbon composite, (3) a carbon/SiC composite, and (4) a SiC/SiC composite. The decision to concentrate on the tungsten armored ferritic was based on the high melting temperature of tungsten, the well understood material properties of both tungsten and steel in a nuclear fission environment, the compatibility of the steel with most all types of coolants, the considerable experience in forming and fabricating these materials, the ability to engineer a tungsten first wall to alleviate some of the more challenging threats, and, arguably the most important, the ability to address most of the critical issues in the short-term with existing facilities and modeling capabilities.

There are three primary challenges with the tungsten armored ferritic:

1. Long term thermo-mechanical fatigue, due to the cyclic heating of the wall.
2. Exfoliation, caused by the entrapment of helium. The helium coalesces into bubbles, because their high energy from the fusion reaction drives them into the wall material, but their short migration distance prevents them from coming out.
3. Development of a high cycle, high thermal conduction bond between the tungsten and the ferritic steel.

The research to address these challenges is the subject of this series of papers in this JNM Special Issue in the Journal of Nuclear Materials. The methodology of our research is as follows:

1. Use target design simulations to determine the emissions incident on the wall (the 'threat spectra').
2. Perform exposure experiments on representative first wall materials to determine the effects of these emissions. The exposures are made with X-ray, ion or other sources that serve as a surrogate for the expected fluence, pulse shape, heat load and spectrum of an actual target. The exper-

iments are backed with modeling. These experiments will bring to light the outstanding issues.
3. Perform the research and development needed to develop materials and configurations that resolve the outstanding issues.

This introductory paper puts the papers in this JNM Special Issue within the context of the overall plan to develop laser fusion energy. In Section 2 we present an overview of the progress and remaining challenges in the development of the other components in a Laser Fusion System. This includes the target design, the lasers, the final optic, target fabrication and target injection. In Section 3 we discuss the factors that must be considered in the design of the reaction chamber. These include the threat spectra to the first wall, the constraints imposed by the laser propagation, target injection, and target tracking, and the requirement for an economically efficient and viable system. In Section 4 we discuss the critical issues in the development of the tungsten armored ferritic wall and the research to address them. These topics are covered in detail in the accompanying papers in the JNM Special Issue, and the material presented here should be regarded only as a coarse summary. In Section 5 we discuss issues that are directly related to the development of the first wall material, including compatibility with blanket concepts, safety and radiological considerations, and long term structural factors.

2. Progress in the development of laser fusion energy

2.1. Target design

For a practical fusion energy power plant, the 'gain' of the target must be greater than 100 in order to balance the projected 6–7% efficiency of the laser system. Here, gain is defined as the energy released by fusion reactions divided by the laser energy onto the target. Projections of the target performance based on 2-D modeling exceed this requirement and predict gains greater than 160 [3]. These simulations are based on the NRL FAST series of codes [4] that have been benchmarked against experiments on the NRL Nike Laser facility [5]. These high resolution simulations model the entire implosion from beginning to end, account for many of the non-uniformities in both the laser and the target, and include all the relevant modes. Such complete simulations are important, as current laser facilities do

not have the energy required to reach ignition, much less high gain. The hardest challenge in any direct drive implosion is the stabilization of Rayleigh Taylor hydrodynamic instabilities that naturally arise because the hot, lower density, ablated material is compressing the cold, higher density, fuel. Modeling has shown that the keys to achieving high gain with the required high stability are the following:

1. Shape the laser pulse so it has a single high intensity 'picket pulse' followed by a low intensity 'foot', followed by a rise to maximum intensity.
2. Make the ablator from a low density foam with DT wicked into it. The foam significantly increases the laser absorption.
3. Preheat the ablator by some means (shocks, X-rays, or a combination). This raises the isentrope of the ablator, and hence lowers the growth rate of the Richtmyer–Meshkov instability. In some designs the ablator is preferentially heated, while the fuel remains on a lower isentrope. This increases the stability without substantially reducing gain.
4. 'Zoom' the laser so the spot size is decreased in radius to match the compressing target. This increases the coupling efficiency of the laser light to the target.
5. Include a thin high Z layer (such as Pd) outside the target. This has been shown experimentally to substantially reduce the imprint of laser non-uniformities, and hence mitigates the seeding of hydrodynamic instabilities [6].

An example of a high resolution calculation of an implosion is shown in Fig. 2. The laser pulse shape is shown in the upper part of the figure. In this case the gain of the target is 160, and the total yield from the target is 400 MJ.

Similar gains have been obtained in single mode calculations from LLNL [1] and the University of Rochester [7].

2.2. Lasers

Two types of lasers are under development: The Krypton Fluoride (KrF) Gas Laser, and the Diode Pumped Solid State Laser (DPSSL). Both of these are being developed with technologies that can be scaled to an IFE sized system.

2.2.1. KrF Lasers

KrF development is carried out on the Electra Laser Facility at NRL (see Fig. 3). A KrF laser uses high voltage (500–800 keV), high current (100–500 kA) short pulse (100–600 ns) electron beams to pump a gas cell filled with Kr, F_2, and Ar. The fundamental laser wavelength of 248 nm is in the ultraviolet, which is required by the direct drive target designs described in Section 2.1. The laser gas, which is slightly above atmospheric pressure,
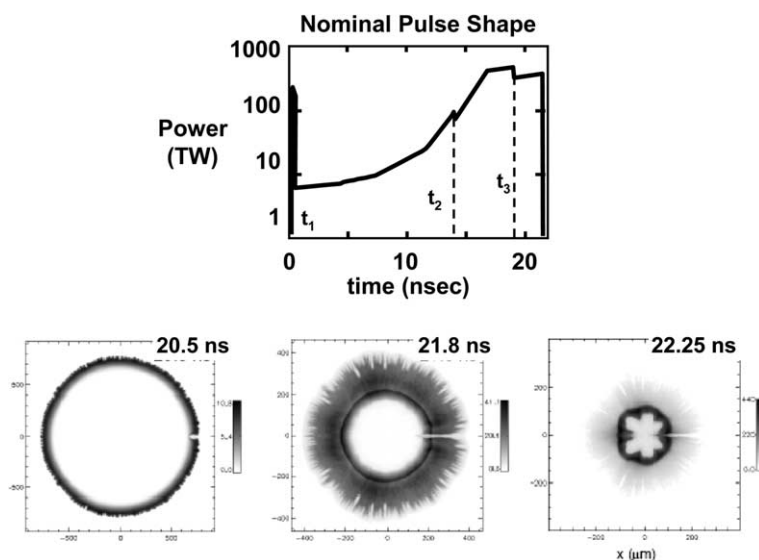
Fig. 2. Pulse shape (upper) and implosion simulations (lower) of a high gain implosion. Dashed lines in the pulse shape show the zooming times. From Ref. [3].

Fig. 3. The electra laser facility.

Fig. 4. The mercury diode pumped solid state laser.
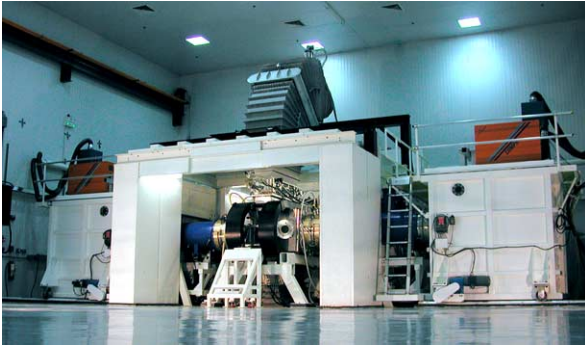
is isolated from the electron beam diode, which is in vacuum, by a foil that is supported by a structure called a hibachi. A recirculator cools and quiets the laser gas. To date Electra has operated as a laser oscillator and produced 400–700 J of laser light at repetition rates of 1 Hz and 5 Hz in bursts ranging from several hundred shots to over 5000. The intrinsic efficiency is 10% in this oscillator mode, which translates to greater than 12% when operating as an amplifier. A new high transmission hibachi has been developed in which the electron beam is configured to miss the hibachi support structure. The new hibachi, along with recent advances in electron beam transport, has increased the electron energy deposition efficiency into the gas from 35% to almost 80%. A new solid state pulsed power switch has been developed which will become the basis for an efficient (>85%), durable, and cost effective (<\$10.00/electron beam Joule) pulsed power system. Based on these results with the key components, the overall efficiency of a full scale system is projected to be greater than 7%. This efficiency, taken in conjunction with the gain 160 targets described in Section 2.1, should meet the requirements for a fusion energy system. KrF lasers have also demonstrated, albeit on a single shot basis, the laser beam spatial uniformity required by the direct drive targets. The durability of the hibachi is the outstanding issue to be resolved in Phase I. This is primarily a thermal management problem, and promising results have been obtained by periodically deflecting the laser gas to cool the foil. Further details on KrF laser development can be found in Ref. [8].

2.2.2. Diode pumped solid state laser

The diode-pumped solid-state laser (DPSSL) approach is being demonstrated with the Mercury laser at LLNL (see Fig. 4). This is a new laser archi-

tecture specially tailored for the fusion application. It can be scaled to an IFE system. The diode arrays are wavelength tuned, spatially smoothed and focused into a stack of seven Yb:S-FAP crystalline amplifier slabs. The collinear optical arrangement of diode light and the laser beam through the crystals maximizes the pumping and extraction efficiency. The crystals are held in aerodynamic vanes to allow distortion-free cooling by high speed helium gas.

The Mercury architecture has required the development of several new technologies: (1) diode array packaging, (2) Yb:S-FAP crystal growth and finishing technologies, (3) a gas-cooled laser architecture and (4) a thermally compensated Pockels cell. The diode bars are assembled on precision manufactured silicon with fiber lenses that optically condition the output radiation. This technology was specifically targeted for an IFE system (high peak power, low duty factor, mass production, and low cost), but is now being developed for other laser applications. The Yb:S-FAP growth process has been improved to produce boules of sufficient size to harvest two full-size laser amplifier slabs, doubling the previous yield. Precision magneto-rheological finishing of the slabs and high damage threshold coatings have been developed to increase the laser damage threshold by a factor of five. The gas cooling is accomplished by compactly arranging the Yb:S-FAP slabs within aerodynamic aluminum support structures to allow face cooling by high speed (0.1 Mach) helium gas. This arrangement allows for 10 Hz repetition rates and excellent thermal management. To keep unwanted stray beams and reflections in check, a full aperture thermally

compensated Pockels cell was developed. All these advances have led to a laser architecture that is more compact and reliable than in previous systems.

Although the entire system is not yet complete, to date the Mercury Laser has simultaneously achieved 4% efficiency (at the 1053 nm fundamental wavelength) at 23 J and 5 Hz for 10^4 shots with <20 ns pulse lengths. Single shot energies reached 34 J and 1 Hz continuous runs with no damage to the system were tested at 10 J and 10 Hz. The goals are to operate at 10 Hz and 100 J with an overall efficiency of 10%. When the frequency is tripled and the beams are smoothed as required by the target design, the efficiency is predicted to be around 7% (which, as pointed out above, should be sufficient for IFE). This performance should be demonstrated in Phase I. Further details on diode-pumped solid-state laser development can be found in Ref. [9].

2.3. Final optics

The final optics steer the laser beams to target center. They are the only optic to lie in the direct line of sight of the target. Their development represents the biggest challenge in the optical train, as they must not only have the high laser damage thresholds required of the other optical components, they must also be resistant to the target emissions. We have developed a final optic concept based on a grazing incidence aluminum surface bonded to a stiff cooled substrate. The substrate is made of a material that is resistant to deformation under neutron irradiation. An example of such a material is SiC. Experiments have shown that a 50 μm optical quality aluminum coating can meet the reflectivity requirements of >99%, and retain the high optical quality requirements for >100 000 pulses at laser fluences of 18 J/cm^2 [10]. Based on this, we believe that this mirror will meet the fluence requirements of 5 J/cm^2 for 10^8 pulses. The remaining challenges for Phase I are to demonstrate this performance on a larger scale system (laser beams spots of a few cm diameter rather than the present few mm), establish a credible technique for creating such an optic (including bonding the aluminum to a suitable substrate) and address the resistance to the target emissions. Regarding the target emissions, preliminary studies show the ions can be magnetically deflected before they reach the optic. The anticipated X-ray fluence at the optic (approximately 0.4–1.0 J/cm^2) is below the damage threshold for single shot events. Studies to determine the effect of long term repetitive X-ray exposures are underway.

2.4. Target fabrication

The current base target design calls for a foam shell, with a density of 100 mg/cc, a diameter of 4.75 mm, and a wall thickness of 250 μm. The foam is filled with deuterium-tritium (DT) ice ($T = 18$ K). The DT layer extends radially inward past the foam for another 330 μm. The foam has an outer solid overcoat of 5 μm pure CH to serve as a vapor barrier to prevent the DT from sublimating. The target will probably also have a thin (50 nm) layer made of a high Z material (Au or Pd) on the outside of the CH barrier. The entire target may also be encapsulated by 4 μm thick, 100 mg/cc empty foam layer. This thermally insulates the cryogenically cold target as it is injected into the hot chamber. A typical target design is shown in Fig. 5 [11,12].

Progress has been made in developing techniques to fabricate this target. Foam shells have been made that have the required diameter, density and wall thickness. Their non-concentricity is less than 5.0% which is within a few of the required 1.0%. An overcoat has been applied to these shells with close to the required smoothness (50 nm RMS, vs the required 20 nm) [13]. These shells have been made with a continuous process that controls the overall diameter within 0.8%. A Pd-Alloy coating has been developed that meets the target physics requirements, has the right permeability for DT (to allow
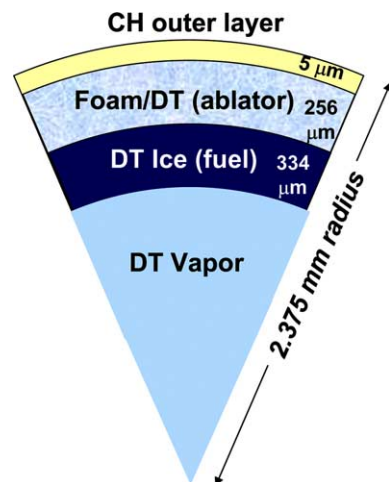
Fig. 5. Sector of a typical target high gain design [11,12].

the target to be filled) and the high infrared reflectivity to help protect the target during injection [14]. Experiments on half scale samples have shown that a DT ice layer grown over a foam underlay can produce the ultra smooth (sub-micrometer RMS) surface layers required by the target physics. (In fact these are much smoother than DT ice layers grown without a foam underlay.) It has also been established that DT layers grown over foam are less sensitive to temperature variations than pure DT layers [1]. This aids in both target handling and target injection. Finally, using established chemical plant costing models, the cost for fabricating and injecting these targets has been estimated to be around $0.16 each [15], which is below the $0.25 required by power plant studies [2]. The remaining challenges in Phase I are to make foam shells that meet the non-concentricity requirements, to demonstrate the enhanced DT ice layering on full scale samples, and to develop a technique for filling and smoothing these layers on a mass production basis.

2.5. Target injection

A repetitively operated target injection facility, based on a light gas gun, has been brought to operation [16]. This facility is being used as a platform to develop technologies for target injection and tracking. An extension at the end of the injector mimics the target chamber. The injector has accelerated surrogate targets to the anticipated required velocity of 400 m/s. Experiments have verified the concept of a separable sabot. The sabot protects the target under acceleration, but then separates into two halves while it is still in the injector barrel. The sabot halves are mechanically deflected into a catcher before they reach the point at which they would be injected into the chamber. The system fires in three shot bursts and typically places the target within ±10 mm of the equivalent center of the target chamber. This is within a factor of 5–6 of the ultimate requirement. The outstanding tasks to complete Phase I are to develop the technology required to meet the placement specifications, and to develop techniques to track the targets inside the chamber.

3. Reaction chamber design constraints

The reaction chamber must serve two major functions: Before the shot it must provide a suitable environment for the target to be injected into the chamber and illuminated with the laser beams. This must be done with the precision needed to achieve the high yield needed for energy production. After the shot the chamber must collect the energy released from the target and provide a means to efficiently extract it for transport to an electricity generator. These functions must be performed 500 000 times per day.

The chamber must be sized so that the flux of target emissions absorbed by the wall (the 'threat spectrum') is below the threshold for mass loss. The threat spectrum consists of X-rays and ions. (The first wall is range thin to the neutrons.) The paper by Raffray et al. in this special issue [17] gives the threat spectra for a typical IFE target. To summarize here, about 1–2% of the target energy output is in X-rays, with half of them having energies above 30 keV. Charged particles comprise 30% of the energy, and the neutrons the balance. The DT fusion reaction produces 3.45 MeV alpha (He^4) particles. These alpha particles are born deep inside the target. As they expand rapidly outward they impart some of their energy to the surrounding 'unburnt' ions (e.g. hydrogen, carbon, deuterium, tritium, etc.). These ions gain energy, and the fusion produced alpha particles loose energy. Thus the alpha spectrum, nor that of the other ions, is no longer monoenergetic. That energy spread allows time us to use time of flight dispersion to greatly reduce the instantaneous threat to the wall.

The threat spectra can be used to calculate the response of the chamber wall, and from that design a reaction chamber. At first blush, one might be tempted to design a chamber that is as large as possible. Another tempting solution is to put a background gas in the chamber to absorb the emissions before they get to the wall [2]. However these options stress target injection and placement, laser focusing, energy conversion in the blanket, and overall economics [1]. Therefore it is best to make the chamber as small as possible.

As an example, we consider a chamber that is 10.75 m in radius and a target energy of 350 MJ. The initial temperature of the tungsten wall chamber is 500 °C, and there is initially no gas in the chamber. These conditions are compatible with target injection into the chamber, high thermal efficiency and candidate blanket designs. Fig. 6 shows the time history of the temperature at various depths in the tungsten wall. The average X-ray fluence on the wall is 0.25 J/cm^2 and the ion fluence is 5.0 J/cm^2, but the calculations were carried out
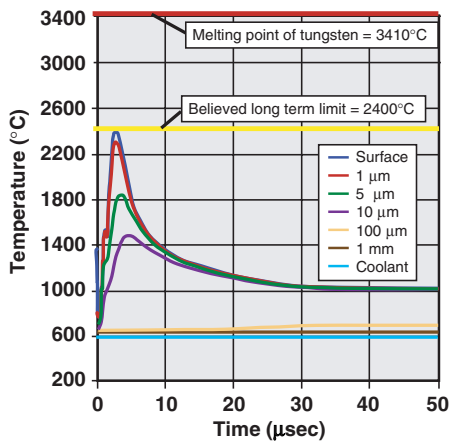
Fig. 6. Tungsten wall temperature profiles for a 10.75 m radius chamber, 350 MJ target.

using the actual spectra. The energy deposition in the tungsten armor was first calculated for a 1-D slab geometry based on photon attenuation calculations (including photo-electric and Compton scattering effects), and on ion energy deposition (including both electronic and nuclear stopping powers). The photon calculations were performed using the methodology described in Ref. [18]. An interactive program based on these calculations can be found at http://aries.ucsd.edu/LIB/PROPS/PHOTON/. The ion stopping was calculated using an interactive program called SRIM (Stopping and Range of Ions in Materials) which may be found at http://www.srim.org/. The underlying physics is discussed in Ref. [19]. The calculation procedure included the time of flight spreading of the photon and ion energy deposition [20]. The thermal analysis was then carried out using a 1-D model including melting and evaporation [20]. Temperature-dependent properties were utilized for the tungsten. Several features can be noted from Fig. 6:

1. The X-ray deposition is very fast, and the wall temperature rapidly rises to 1150 °C from an initial temperature of around 500 °C. The wall cools down substantially (nearly to its starting temperature) over the next 400 ns, and then rises to a second peak at ~2900 °C due to the ions. Thus the temperature is always below the tungsten melting point of 3410 °C.
2. This behavior is only possible with a target that does not produce copious X-rays. For an indirect drive target, in which an outer hohlraum converts a significant amount of the alpha and burn

ion energy to X-rays, the X-ray yield is more than ten times greater than a direct drive target with the same yield. Thus the initial X-ray pulse would drive the wall well past the melting point, and a solid wall chamber is not an option with an indirect drive target.
3. Most of the heating takes place within a very thin (~30 μm) region from the surface. This is why we can separate the functions of the first wall into an armor that is resistant to the target emissions, and an underlying substrate to provide the supporting structure and interface with the blanket. (Note the blanket effectively sees steady-state conditions.)
4. The first wall returns to its initial 500 °C within several hundred microseconds, i.e. well before the 200 ms inter-shot time.

Note that if additional thermal protection of the target is required, calculations show this can be attained by encasing the target with a thermally insulating foam shell, 100 μm thick, with 100 mg/cc. The foam does not compromise the performance of the target, according to both 1-D simulations using the same code used in Fig. 2 [21] and single mode 2-D simulations [22]. Further details on the threat spectra, design limits and operating windows are given by Raffray et al. in this JNM Special Issue [17].

4. Critical issues for a tungsten armored first wall

The previous section showed the tungsten wall will not melt after each shot. While this is certainly a necessary criterion for the energy application, it is not the only one. We must also consider long term cyclic issues. For the tungsten/steel structure we are evaluating these are: long term cyclic fatigue, helium retention, and long term bond integrity.

4.1. Long term cyclic fatigue

To study cyclic fatigue, we have exposed tungsten to X-rays and ions at IFE relevant pulse lengths, energies, and fluences. (In experiments to date we have used powder met tungsten. In the actual application we expect to use CVD tungsten in order to bond the tungsten to the steel. However for the first experiments we wanted to start with a material with a well established morphology.)

X-ray exposures are carried out on two facilities: The Sandia Z facility [23] is a single shot machine

capable of exposing a sample with X-ray energies of ~1.5 keV and fluences in excess of 60 J/cm². This is more than 50 times the anticipated wall loading. For multiple exposures, we use the XAPPER facility. As discussed in the JNM Special Issue paper by Lat-kowski et al. [24], this is a repetitive (10 Hz) X-ray source capable of exposing samples with fluences up to 1 J/cm² (X-ray energy 100–150 eV) for large numbers of pulses. The system is capable of running 10^6 pulses continuous. Ion exposures are carried out with the RHEPP-1 Facility at Sandia [25]. RHEPP-1 is capable of exposing samples with 500–900 keV ions (singly charged helium, neon, nitrogen, etc.) at fluences up to 8 J/cm², pulse lengths of up to 100 ns, and repetition rates approaching 0.1 Hz. Exposures of more than 1000 pulses are possible. These studies are discussed in the paper by Renk et al. [26].

The results for X-ray exposures on Z and ion exposures on RHEPP are shown in Table 1. From these results, X-rays do not appear to be a problem. The paper in this JNM Special Issue by Tanaka et al. [27] reports experiments with Z show no effect with X-ray loading up to 2.3 J/cm², which is well above the estimated wall loading. Above that tungsten shows signs of roughening. At higher fluences the tungsten starts to melt. These are single pulse results, and while they are encouraging, we need to make sure there are no long term thermo-mechanical fatigue issues. Hence the experiments on XAPPER as reported in Ref. [24]. In contrast to the X-rays, ions may be a problem.

In the column in Table 1 titled 'Predicted Threat to the IFE Wall', the first number in each of the ion boxes is the predicted total fluence on the wall for an IFE target. These ions are incident on the wall in a double humped distribution spread over 2.1 μs FWHM. On the other hand, the ions from RHEPP-I are incident on the sample in a pulse of approximately 100 ns FWHM (although this varies slightly with the ion species). The numbers in parenthesis are adjusted to allow a more reasonable comparison between the RHEPP-1 fluences and those expected in an IFE chamber. They are obtained

by applying a $t^{1/2}$ correction for the pulse width. This scaling is only an approximation, as its validity depends on several factors (such as the ratio of the thermal diffusion length to the energy deposition length). Note that we are well below the ablation threshold for tungsten. But we are close to the roughening threshold. In fact the paper in this JNM Special Issue by Renk et al. [24] reports that the roughening, as measured by the surface finish, does not seem to saturate even after 1000 pulses. What has not yet been established is if this roughening is a problem or not ... in other words does it lead to mass loss, or cracks that penetrate all the way to the substrate, or does the process eventually saturate? These issues are addressed in both JNM papers by Renk [26] and Blanchard and Martin [28].

We have also set up a laser exposure facility to mimic the effects of X-rays and ions on the first wall material. Calculations show that a properly shaped laser pulse can match the steep temperature deposition profile in the first wall shown in Fig. 6. Thus the laser should be capable of duplicating all the relevant temperature-dependent mechanisms with the exception of those due to the initial temperature transient or outright ablation. (This will be verified with direct comparison with the same material exposed to either ions or X-rays.) This approach is advantageous because a laser can fire for large numbers of pulses at high repetition rate in an environment that is more 'diagnostic friendly' than an ion or X-ray device. For example, this facility has a precisely calibrated optic thermometer that can measure the real time temperature behavior of the exposed surface. In preliminary experiments with 10 000 shot runs, with the fluence sufficient to bring the tungsten temperature up to 3000 °K (i.e. just below melting), the response of the tungsten was qualitatively similar to what was observed with the ion experiments: the surface was observed to roughen [29].

The roughening is believed to be due to cyclic thermo-mechanical fatigue. The surface heats up when expose to the ions, but cannot expand against the cool underlying layer. The resulting strain

Table 1
Results of exposure of powder met tungsten to X-rays and ions

Threat	Analytic predicted ablation threshold	Measured ablation threshold	Measured roughening threshold	Predicted threat to wall
				350 MJ target (10.75 m radius)
X-rays (10 nsec exposure)	2.4 J/cm³	2.3–19 J/cm²	2.3 J/cm²	0.25 J/cm²
Ions (~100 nsec exposure)	5.1 J/cm³	6 J/cm³	1.25 J/cm²	4.99 J/cm² (1.11 J/cm²)

results in a compressive stress that exceeds the material strength. As discussed in the JNM Special Issue paper by Blanchard and Martin [28], fatigue modeling indicates that surface cracks can be expected to appear within a few thousand cycles of operation, depending on the target yield, chamber size, and chamber gas pressure. Hence, the design must tolerate these cracks. If the cracks are prevented from propagating to the steel or along the interface, then the wall should survive the requisite number of pulses without tungsten delamination or failure of the underlying structure. Fig. 7 shows the stress intensity as a function of crack half-spacing for 50 and 75 μm deep cracks in a 250 μm layer of tungsten. This demonstrates that for a half spacing of 50 μm (distance between cracks of 100 μm), the stress intensity drops to 0 and crack growth will stop. Hence, a 250 μm thick layer of tungsten, castellated with spacing on the order of 100 μm, should prevent cracks from propagating to the steel and thus should provide a viable wall design. Calculations are under way to explore the behavior of deeper cracks with larger spacing.

As pointed out in the paper by Snead et al. such an engineered structure would be straightforward to realize, and would not appreciably affect the known material properties of the tungsten [30]. A more radical approach would be to use a micro engineered armor consisting of either tungsten foam or plasma sprayed tungsten. This research is described in the paper in this JNM Special Issue by Sharafat et al.
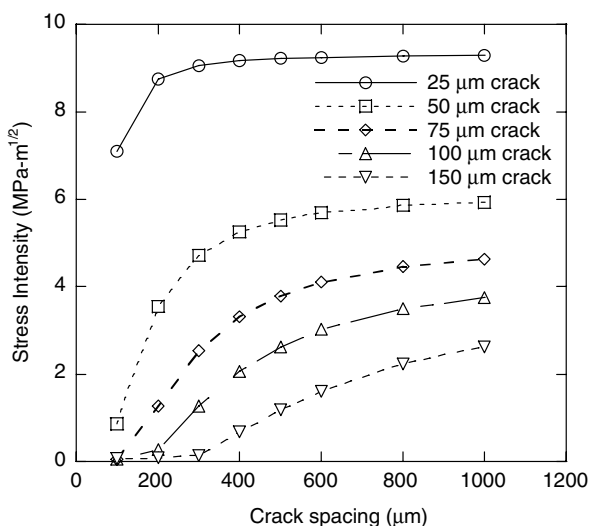
[31]. The idea is the same as with the castellated structure i.e. allow unrestricted thermal expansion and contraction of the armor. As the size is probably smaller than what we would require, such a measure would probably not be employed if thermo-mechanical fatigue were the only issue. As discussed below, these micro-engineered armors may also help mitigate helium retention.

4.2. Helium retention

The alpha particles embed themselves several microns into the tungsten because of their high kinetic energy. However once they are implanted, they get trapped in defects such as vacancies and grow into bubbles. The migration distance of helium bubbles at 850 °C is only 20 nm, as determined by TEM analysis. Continued helium implantation results in growth and coalescence of these bubbles which eventually cause the material to blister and exfoliate. For example, for the anticipated flux of 2×10^{18} He/m^2 s, it is estimated that this process will remove about 2 cm/year from the wall. This is unacceptable, as the initial tungsten armor would be less than a few mm thick. This effect has been observed and well documented under MFE conditions [32]. The scope of this challenge has led us to attack the problem with two complementary approaches. The first, and most obvious, is to establish if this really is a problem in an IFE system, where the wall temperature is initially higher, the temperature gradients are much steeper, and implantation in the tungsten armor is followed with a spike in temperature to up to 2000–3000 °C (see Fig. 6). The second approach is to investigate and develop advanced micro-engineered materials that have typical feature sizes less than the classical helium migration distance.

In the first approach, experiments and modeling of tungsten implanted with helium at IFE conditions are reported in the JNM Special Issue papers by Snead et al. [33] and Parikh et al. [34]. In these experiments helium ions of the right energy spectra are produced by a Van de Graff Accelerator and implanted into a tungsten sample. Nuclear depth profiling (NDP) and nuclear reaction analysis (NRA) has been performed to measure the retention of helium as a function of implantation packet (ion dose) and annealing temperature. Results from the first experiments with a mono-energetic source of helium are shown in Fig. 8. The figure on the left shows the exposure history of repetitive cycles of

Fig. 7. Predicted stress intensity as a function of crack half-spacing a 250 μm layer of tungsten, chamber radius of 7 m, and a 150 MJ yield target.
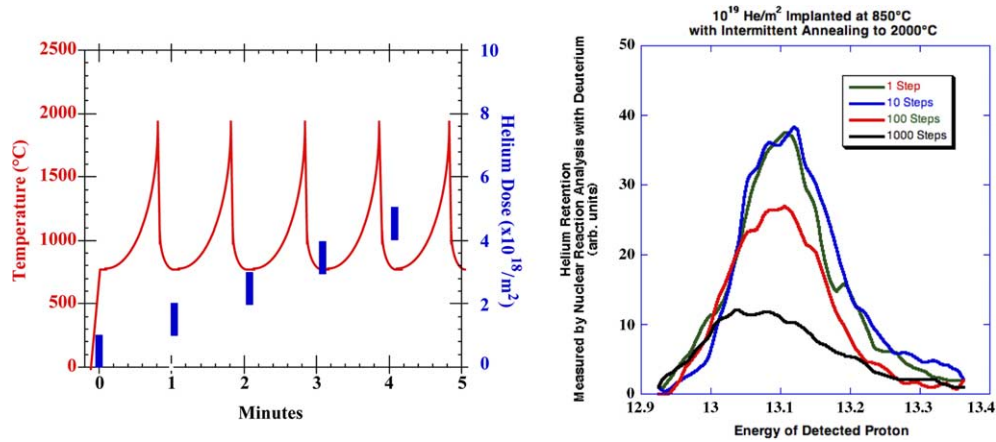
Fig. 8. Exposure history and measurement of retained helium. Note that as the exposures get closer to typical IFE Chamber first wall conditions, the retained helium decreases.

1.3 MeV helium implanted with 2000 °C annealing between exposures. The figure on the right shows the results of the retention (NRA analysis) clearly indicating that as the ion packet size is reduced (for constant total dose) the retained helium is significantly reduced. Modeling is being carried out by application and upgrade of the MODEX code developed by DELFT in the Netherlands [35], as well as the HEROS code developed at UCLA [31]. The latter combines SRIM to calculate radiation damage, kinetic rate theory to simulate the helium bubble evolution, and classical diffusion theory to track helium through the tungsten structure. The preliminary conclusion is that retained helium is far less of a problem under IFE conditions. Still to be resolved are understanding the effects of implantation/anneal cycle times that are closer to IFE conditions, and the effects of vacancies caused by neutron damage.

In addition to these efforts, there is also a program to implant helium and hydrogen into tungsten using an electrostatic trap. The samples can be operated at prototypical IFE temperatures and fluences. However, the ion source is continuous, and the energy is only 30 keV, so the parameters are different from the expected IFE conditions. These experiments will allow simultaneous exposure to both helium and hydrogen ions, and are expected to give fundamental insight into the nature of helium retention in solids. Details of this work are reported in the paper in this JNM Special Issue by Cipiti [36].

The second approach is to develop a micro-engineered armor whose characteristic feature size is less than the classical helium migration distance. Two types are under consideration. One is a tungsten foam, the other is a tungsten layer applied by a vacuum plasma spray process. In both concepts the armor is porous, with the plasma sprayed armor having feature sizes on the order of a few tens of nm and the foam having ligaments of 10–20 μm in diameter. As pointed out in Section 4.1, these small sizes should also mitigate damage due to cyclic thermo-mechanical stresses. The key questions about these designs, other than the obvious ones of will they show the intended advantages, is that little is known about the fundamental properties of these materials, including thermal conductivity, bonding, and X-ray and ion damage threshold.

The experimental and theoretical research program to address these issues is presented in the JNM Special Issue paper by Sharafat [31]. This includes both development of the armor and the appropriate modeling. As an example of the latter, consider the most obvious question, the transfer of heat from the foam to the underlying structure. A 3-dimensional transient structural analysis was used to determine the dynamic response of the structure. In response to the combination of static internal coolant pressure and transient external pressure on the face of first wall modules, time-dependent displacements, strains, stresses, and forces were obtained. Fig. 9 shows the results of the analysis. The maximum calculated Von Mises stresses are of the order of 4 MPa, which is well below the allowable stress for low activation ferritic steel of 148 MPa at 500 °C.

A thermal analysis was performed on a 20 μm thick tungsten coated composite steel substrate. In
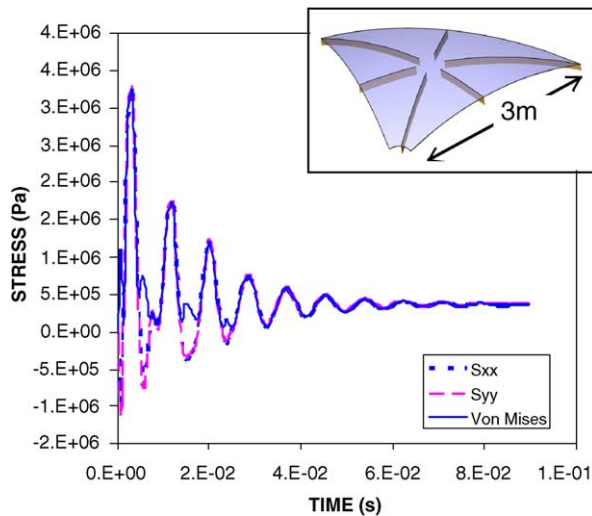
Fig. 9. Transient dynamic response of a 3-mm thick FW LAFS steel section with supporting ribs (inlay) following a single pressure pulse.

Fig. 10. 3-D Solid model of W-foam armored FW (right); thermal transient analysis results of a single pulse (left).

this case the 2-mm thick low activation ferritic steel (LAFS) is attached to a 1-mm thick oxide dispersion strengthened (ODS) reduced activation ferritic/martensitic steel. The coolant at the back of the LAFS is assumed to be 400 °C, and the transfer coefficient is assumed to be 10000 W/m² K. The tungsten layer thickness was varied between 1 and 50 μm. The maximum tungsten surface temperature reaches an asymptotic value of 2800 °C (W melts at 3400 °C) with a layer thickness of 20 μm. Furthermore, the W/ODS interface temperature reaches a minimum value of 500 °C with a W-thickness of 20 μm. This implies that a tungsten armor thickness of 20 μm would be sufficient to protect the main ODS ferritic structure from the high temperature transient at the FW surface.

A 3-D thermo analysis was performed on the tungsten foam armor on the composite steel substrate (2-mm thick LAFS on 1-mm thick ODS) with a cooled back under the same conditions as above. A 3-D solid model of the tungsten foam was constructed with 20 μm thick and 80 μm long square ligaments. The total height of the foam of 0.8 mm was chosen to prevent any direct line of sight to the steel substrate. Ligament surfaces were illuminated selectively, based on the shadowing of deeper lying ligaments. Thus the top ligament surfaces are completely exposed, while illuminated surfaces become increasingly smaller towards the steel substrate. Fig. 10 shows the results of this analysis.

The exposed ligament surfaces reach a maximum temperatures value of 2800 °C, however deeper in the foam the heated areas of exposed ligaments decreases with depth towards the steel substrate. Thus the energy is deposited quasi-volumetrically deep into the armor, instead of being absorbed solely within the top 5 μm of a solid tungsten coating. This quasi-volumetric heating of the foam spreads the energy deposition over a larger volume and may alleviate the thermal stresses of a bulk tungsten coating. The analysis shows the transient thermal behavior of the foam to be similar to that of the bulk tungsten coating with the W-LAFS interface reaching a maximum of 545 °C and returning to 500 °C before the next pulse.

4.3. Long term bond integrity

The third major critical issue is the development of a high thermal conductivity bond that is resistant to deep-cycle thermo-mechanical fatigue. Although the temperature is approximately steady state within 100 μm of the armor surface, there are still temperature swings and hydrodynamic shocks in effect at the interface.

As discussed in the JNM Special Issue paper by Snead et al. [30] experiments have investigated the application of tungsten armor to low activation F82-H ferritic-martensitic steel. The tungsten armor thickness was 100 μm. Three processing routes were evaluated for applying a 100 μm layer of tungsten to the F82-H: diffusion bonded W, powder transient melt, and plasma spray. All three approaches yielded uniform coating of tungsten on the steel, although the most uniform coatings were achieved by plasma spray and diffusion bonding.

A separate paper in this JNM Special Issue [37] describes studies to apply 100 μm of tungsten to silicon carbide (Hexoloy SiC). This is another first wall concept. This has been achieved by melting a powder mixture of tungsten and other additives with the Plasma Arc Lamp InfraRed Processing Facility at ORNL [38].

Testing of these tungsten armored materials showed similar properties. In both cases a uniform, fully-dense tungsten layer was formed. Conventional bend testing showed that delamination did not occur prior to sample failure. And in both materials failure in the base material occurred prior to spallation of the tungsten coating. A series of thermal fatigue tests were carried out using the InfraRed Processing Facility. The heat flux and duration was chosen to mimic the interfacial stresses expected in the actual first wall. A 600 °C base temperature was chosen. For the W/F82-H steel the heat load was 20.9 MW/m^2 of duration 20 ms, for 1000 pulses. For the W/ SiC the corresponding numbers were 23.5 MW/m^2 for 10 ms, again for 1000 pulses. In both cases no spallation or cracking at the interface was observed. These studies have been supported by the thermo-mechanical modeling efforts presented in the paper by Blanchard and Martin in this JNM Special Issue [25].

It is realized that applying the armor by any of these techniques might alter the thermo-physical properties of the tungsten. Thus, after a satisfactory bond has been achieved, it is then necessary to ensure that the resulting armor still meets the requirements for damage threshold, fatigue, thermal conductivity, and helium retention.

5. Other first wall issues

There are three other considerations that must be taken into account in the development of a viable first wall: Compatibility with the blanket, safety and radiological issues, and structural considerations.

5.1. Compatibility with blanket concepts

As shown in Fig. 6, only a thin region of the armor (10–100 μm) will experience the highly cyclic energy deposition transients from the target microexplosion. The first wall structure behind the armor as well as the blanket will operate under quasi-steady-state thermal conditions, very similar to MFE conditions. This allows the possibility of making full use of information from the large international MFE blanket effort in adapting a blanket for the laser IFE case. The blanket would have to be compatible with the choice of ferritic steel (FS) as structural material and to provide adequate performance under coolant temperature constraints dictated by FS and tungsten armor maximum temperature limits.

Potentially attractive blanket concepts for IFE include: self-cooled Li; He-cooled ceramic-breeder; He-cooled or dual cooled Pb–17Li, and dual cooled molten salt (with He as FW coolant). In general, it is desirable to compare a Rankine steam cycle with a Brayton gas cycle in order to select an optimized power cycle for each blanket. However, other considerations also influence the cycle selection; for example, for the Li-cooled blanket, it is strongly desirable to avoid any possibility of Li/steam accidental reaction and a Brayton cycle is preferred.

The maximum temperature constraint for FS depends on the local stress conditions but can be assumed to be 550 °C for regular FS and up to ~700 °C for oxide-dispersion-strengthened (ODS) FS. Other constraints relate to its compatibility with the coolant (other than helium) which would restrict the maximum structure/coolant interface temperature (e.g. ~550–600 °C for Li and ~450 °C for Pb–17Li). Depending on the design configuration and conditions, coatings or inserts as corrosion protection and/or thermal insulation on the FS could help increase the coolant operating temperature and the cycle efficiency. One such example would be to use a SiC insert in the case of the Pb–17Li coolant. However, the gain in performance would have to be balanced against the additional complexity and R&D linked with the utilization of such coatings or inserts.

Another constraint on the coolant temperature is the maximum temperature limit on the tungsten armor. Overall, the coolant conditions must accommodate all the above-mentioned constraints while still providing a reasonable performance through the power cycle. Our initial scoping analysis indicates that such a design window exists providing cycle efficiencies of ~40% or higher. For example, a Li-cooled blanket with an outlet blanket coolant temperature of ~650 °C results in a cycle efficiency >42% with a Brayton cycle. This design accommodates all the constraints without the presence of an insert or coating on the in-chamber FS. More design analysis of the different blanket concepts is required to obtain a better understanding of the operation and performance of each concept in an IFE setting

and to help converge on a choice of the most attractive configuration(s) for a full design study of a laser IFE power plant.

5.2. Safety and environmental considerations

In addition to ions and X-rays, the first wall will see large fluxes of neutrons. Although these neutrons are not stopped in the first wall from the point of view of thermal or thermo-physical considerations, they will eventually damage the material. This radiation damage may limit the useful lifetime of the wall. Depending upon the elemental composition and component lifetime, the neutron activation may be to such a degree that the first wall can no longer be disposed of as Class C waste. In this section, we elaborate upon these issues and provide an estimate of the first wall waste volume.

Because a blanket design has not yet been adopted for use with the tungsten/ferritic steel first wall, we used the parameters developed during the SOMBRERO power plant study [2]. To get the neutron spectrum in the first wall, the carbon first wall in SOMBRERO was replaced with the steel structure considered here. (The tungsten was ignored at this stage because it is so thin.) This spectra was then used to calculate the displacements per atom (dpa) for each year of operation, using the SPECTER code [39]. For a fusion power of 2680 MW and a radius of 6.5 m, the neutron wall loading is $\sim$4 MW/m^2. At this neutron wall loading, the tungsten first wall would experience $\sim$7 dpa/year. (Note that this is less than in an MFE system. This is because the neutron spectra is much softer than in an MFE system. The neutrons are born in the center of the target, and impart their energy to the surrounding mantle of unburnt fuel as they propagate outward. This process was discussed in Section 3.) For a damage limit of even only 50 dpa, the first wall lifetime would be more than 7 full-power years (fpy). Helium production occurs at a rate of 4.5 appm/fpy, which is insignificant compared to the large number of alphas emitted from the direct-drive target.

In order qualify as Class C waste, a component must have a waste disposal rating (WDR) of less than unity. The WDR is calculated as the ratio of the concentration of a given radionuclide to the concentration limit for that radionuclide, summed over all radionuclides. Class C waste would qualify for disposal via shallow land burial, as opposed to deep geologic disposal. While US law does not currently

include limits for most fusion-relevant radionuclides, one can assume that the same methodology used to develop limits for fission-relevant isotopes would be applied for fusion. Fetter [40] did just this, and it is his proposed limits that we use.

A pure tungsten first wall would meet Class C requirements for an irradiation time of $\sim$5 fpy. After that, the concentration of ^{186m}Re would exceed the limit, and the first wall would no longer qualify for shallow land burial. ^{186m}Re is produced via the multi-step reaction/decay chain: ^{186}W(n,γ)^{187}W $\rightarrow$ β^- decay $\rightarrow$ ^{187}Re(n,2n)^{186m}Re.

It is common practice to alloy tungsten with rhenium in order to gain some ductility through a reduction in the ductile-to-brittle-transition temperature. Unfortunately, this accelerates the production of ^{186m}Re and shortens the time at which the material fails to meet Class C requirements. Fig. 11 shows the WDR as a function of irradiation time for pure tungsten and W-3Re, a common alloy. While the pure tungsten wall does not reach a WDR of unity for nearly 5 fpy, the alloyed wall fails to meet Class C requirements in just over 2 fpy. Alloys with higher concentrations of rhenium would fail to meet Class C requirements in even less time.

Even if the first wall fails to meet the Class C requirements for disposal, only a small quantity of waste will be generated. For a first wall that is 1 mm thick, the waste volume is only $\sim$0.5 m^3 per wall change-out. Assuming a useful first wall lifetime of 5 fpy, this adds up to only $\sim$3 m^3 over an expected power plant lifetime of 30 fpy.

If the goal to only produce waste that satisfies Class C requirements is adhered to, a pure tungsten first wall should be replaced at least every 4 fpy.
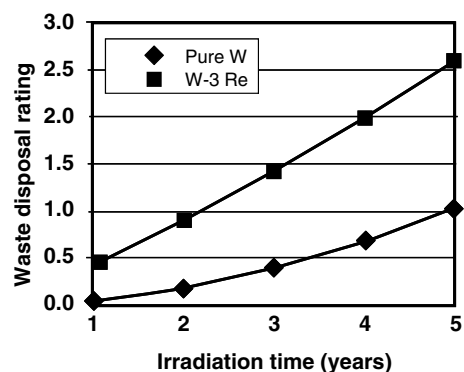
Fig. 11. Waste disposal ratings for pure and alloyed tungsten as a function of irradiation time.

This would generate <4 m^3 of Class C waste over the power plant lifetime. For a tungsten alloy wall, replacement every 2 fpy, or even more frequently, would be required. Even for annual replacements, the first wall waste would amount to only 15 m^3 over the plant lifetime. This is insignificant compared to other sources of Class C waste that would be generated during the power plant lifetime.

Although a detailed power plant design is not yet available, we can still make a few general comments about safety: The currently envisioned operating window calls for a significantly lower gas pressure than that used in the original SOMBRERO design [2] – 25 mTorr maximum vs the original 500 mTorr. Activated xenon gas was a significant contributor in those accident dose calculations [41], thus this factor will be correspondingly be reduced. In addition, the original design used a carbon composite first wall and blanket, which caused tritium retention to be a significant issue. As tritium retention in tungsten is low, and the main blanket will most likely not use a carbon composite structure, the overall tritium retention should be lower, and the overall accident dose should be lower as well. These were among the factors that led to the current choice for first wall.

Due to the relatively short half-life of ^{187}W (23.9 h) and the high energy release per decay, radioactive afterheat is usually raised as a concern when tungsten is used in fusion systems. For some power plant concepts, this afterheat can lead to melting in some accident scenarios. For the first wall discussed here the small amount of tungsten used eliminates this as a concern – the tungsten afterheat is only ∼1 MW, which is small compared to the fusion power that would ordinarily be handled without difficulty.

Safety and environmental considerations will continue to have an effect upon the first wall and blanket designs. Once the program is ready to develop an integrated point design, safety and environmental issues will be evaluated in even greater detail.

5.3. Structural issues

5.3.1. Fatigue and creep rupture

Because commercial laser fusion devices will operate at frequencies on the order of 5–10 Hz, fatigue crack growth in both the tungsten and steel must be considered. The tungsten armor experiences significant plastic deformation during each shot. Plastic strain ranges at the tungsten surface are expected to be 1–3%, depending on the target yield, gas pressure, and chamber radius. Hence, this is in the low cycle fatigue regime and cracking will be expected to initiate after a few thousand cycles [28]. However, this plasticity only occurs within the first few tens of microns of the tungsten. As the cracking progresses away from the surface, the loads decrease and therefore the crack growth rate decreases. Detailed fracture analysis indicates that for sufficiently thick armor coatings (at least 250 μm), the driving force for crack growth vanishes and the crack stops [28]. Therefore, it is possible that the armor coatings will have lifetimes of several years, despite the expected surface cracking after only hours of operation. This remains to be verified experimentally.

The other potential fatigue issue in this wall design is high cycle fatigue at the interface between the tungsten and the steel. However, analysis has shown that as long as there is no plastic deformation in the steel, it will always be in compression and therefore fatigue crack growth is not expected [28].

Creep must also be considered as a possible failure mechanism, because of the high stresses and temperatures involved. Creep rupture analysis in the tungsten is complicated by the fact that the tungsten surface is only at high temperature for on the order of 10 μs, and only the first 20 μm experiences significant temperature excursions. Therefore, creep rupture will only be an issue in the near surface region of the armor. Experiments must verify that extensive creep in the near surface regions of the non-structural armor will not have long term implications for the life of the wall.

In order to prevent failure in the steel by creep rupture, the design must maintain the stress below the design stress. Using data for F82-H, a well-studied ferritic alloy containing 8% chrome and 2% each tungsten, vanadium, and tantalum, the design stress based on creep rupture to ensure a life of 10 000 h is approximately 130 MPa [42]. Given that the first wall is expected to operate around 500 °C, and that the stresses are relatively low with sufficiently thick armor, creep rupture in the steel should not be an issue [28]. The fact that the stresses remain compressive in the steel also helps in this regard.

5.3.2. Irradiation effects: swelling and embrittlement

There is little data available for irradiated tungsten. Based on results for other refractory alloys and limited data on tungsten, one would expect

neutron irradiation to increase the strength and decrease the ductility of the tungsten armor [43]. One would prefer to irradiate the tungsten at temperatures above approximately 900 °C, as the ductility loss is more pronounced below about $0.3T_m$, but this is impossible since the tungsten will be in contact with the steel, which cannot operate at this temperature. Hence, greater understanding of the irradiation of tungsten at temperatures between 700 and 1000 °C is needed [43]. Swelling is not expected to be significant in tungsten (<2% for fluences up to $2–5 \times 10^{26} \, n/m^2$, $E > 0.1$ MeV [43]), though more experiments are necessary to verify this, primarily for a fusion spectrum.

There is significant data on the irradiated properties of ferritic alloys. In general, they are relatively resistant to swelling, but are susceptible to embrittlement, largely through increases in the ductile to brittle transition temperature. This can be alleviated somewhat by operating above about 250 °C, but the minimum temperature may have to be higher when helium (produced by transmutation reactions) is present [44]. Since the steel temperatures in the chamber should exceed 400 °C, this is not likely to be a problem.

6. Summary

We are undertaking a research program to develop the science and technology of laser fusion energy. Significant progress has been made in the lasers, target design, target fabrication and final optics. One of the major remaining challenges is the development of a viable first wall for the reaction chamber. This paper gives an overview of the research on a first wall based on tungsten armored ferritic steel. Details of this research can be found in the articles in this special issue of the Journal of Nuclear Materials.

References

[1] J.D. Sethian et al., Nucl. Fusion 43 (2003) 1693.
[2] I.N. Sviatoslavsky, M.E. Sawan, R.R. Peterson, et al., Fusion Technol. 21 (1992) 1470.
[3] A.J. Schmitt, D.G. Colombant, A.L. Velikovich, S.T. Zalesak, J.H. Gardner, D.E. Fyfe, N. Metzler, Phys. Plasmas 5 (2004) 2716.
[4] M.H. Emery, J.P. Boris, J.H. Gardner, Appl. Phys. Lett. 41 (1982) 808.
[5] A.J. Schmitt, A.L. Velikovich, J.H. Gardner, C.J. Pawley, S.P. Obenschain, Y. Aglitskiy, Y. Chan, Phys. Plasmas 8 (2001) 2287.
[6] S.P. Obenschain, D. Colombant, M. Karasik, C.J. Pawley, V. Serlin, A.J. Schmitt, J. Weaver, J.H. Gardner, L. Phillips, Y. Aglitskiy, Y. Chan, J.P. Dahlburg, M. Klapisch, Phys. Plasmas 9 (2002) 2234.
[7] S. Skupsky, R. Betti, T.J.B. Collins, et al., High-gain direct-drive target designs for the national ignition facility, in: K.A. Tanaka, D.D. Meyerhofer, J. Meyer-ter-Vehn (Eds.), Inertial Fusion Sciences and Applications 2001, Elsevier, Paris, 2002, p. 240.
[8] J.D. Sethian, M. Myers, J.L. Giuliani Jr., R.H. Lehmberg, P. Kepple, S.P. Obenschain, F. Hegeler, M. Friedman, M.F. Wolford, R. Smilgys, S.B. Swanekamp, D. Weidenheimer, D. Giorgi, D.R. Welch, D.V. Rose, S. Searles, Proc. IEEE 92 (2004) 1043.
[9] A.J. Bayramian, R.J. Beach, W. Behrendt, C. Bibeau et al., Activation of the Mercury laser, a diode-pumped, gas-cooled, solid-state slab laser, OSA Trends in Optics and Photonics, vol. 83, Advanced Solid-State Photonics, p. 268.
[10] M.S. Tillack, J. Pulsifer, K. Sequoia, UV Laser-Induced Damage to Grazing Incidence Metal Mirrors, Third International Conference on Inertial Fusion Sciences and Applications (IFSA2003). Monterey CA, Sep 8-12, 2003. Paper WPo4.31. Accepted for publication in American Nuclear Society.
[11] S.E. Bodner, D.G. Colombant, A.J. Schmitt, M. Klapisch, Phys. Plasmas 7 (2000) 2298.
[12] D. Colombant, S.E. Bodner, A.J. Schmitt, et al., Phys. Plasmas 7 (2000) 2046.
[13] D. Carey, J. Streit, Private communication, 2004.
[14] R.W. Petzoldt, D.T. Goodin, A. Nikroo, E. Stephens, N. Siegel, N.B. Alexander, A.R. Raffray, T.K. Mau, M. Tillack, F. Najmabadi, S.I. Krasheninnikov, R. Gallix, Nucl. Fusion 42 (2002) 1351.
[15] D.T. Goodin, N.B. Alexander, L.C. Brown, et al., Nucl. Fusion 44 (2004) S254–S265.
[16] D.T. Goodin, N.B. Alexander, C.R. Gibson, A. Nobile, R.W. Petzoldt, N.P. Siegel, L. Thompson, Nucl. Fusion 41 (2001) 527.
[17] R. Raffray et al., J. Nucl. Mater., this issue, doi:10.1016/j.jnucmat.2005.08.015.
[18] M.J. Berger, J.H. Hubbell, XCOM: Photon Cross Sections on a Personal Computer, National Bureau of Standards, 1987. NBSIR 87-3597.

[19] N. Bohr, Mater. Fys. Medd. Dan. Vid. Selsk. 18 (8) (1948).

[20] A.R. Raffray, D. Haynes, F. Najmabadi, J. Nucl. Mater. 313 (2003) 23.

[21] A.J. Schmitt, Private communication, 2004.

[22] L.J. Perkins, Private communication, 2004.

[23] R.B. Spielman, C. Deeney, G.A. Chandler, M.R. Douglas, et al., Phys. Plasmas 5 (1998) 2105.

[24] J. Latkowski et al., J. Nucl. Mater., this issue, doi:10.1016/j.jnucmat.2005.08.018.

[25] T.J. Renk, P.P. Provencio, S.V. Prasad, A.S. Shlapakovski, A.V. Petrov, K. Yatsui, W. Jiang, H. Suematsu, Proc. IEEE 92 (2004) 1057.

[26] T. Renk et al., J. Nucl. Mater., this issue, doi:10.1016/j.jnucmat.2005.08.021.

[27] T. Tanaka, Private communication, 2004.

[28] J. Blanchard, C. Martin, J. Nucl. Mater., this issue, doi:10.1016/j.jnucmat.2005.08.007.

[29] F. Najmabadi, Private communication, 2004.

[30] L. Snead et al., J. Nucl. Mater., in press.

[31] S. Sharafat et al., J. Nucl. Mater., this issue, doi:10.1016/j.jnucmat.2005.08.012.

[32] W. Wang, J. Roth, S. Lindig, C.H. Wu, J. Nucl. Mater. 299 (1999) 124.

[33] L. Snead et al., J. Nucl. Mater., in press.

[34] N.R. Parikh, S.B. Gilliam, S.M. Gidcumb, B.K. Patnaik, J.D. Hunn, L.L. Snead, G.P. Lamaze, J. Nucl. Mater., this issue, doi:10.1016/j.jnucmat.2005.08.017.

[35] A.V. Fedorov, A. van Veen, Comput. Mater. Sci. 9 (1998) 309.

[36] B.B. Cipiti, G.L. Kulcinski, J. Nucl. Mater., this issue, doi:10.1016/j.jnucmat.2005.08.009.

[37] T. Hinoki, L. Snead, C.A. Blue, J. Nucl. Mater., this issue, doi:10.1016/j.jnucmat.2005.08.020.

[38] C.A. Blue, V. Sikka, E. Ohriner, et al., JOM-e 52 (1) (2000).

[39] L.R. Greenwood, R.K. Smither, SPECTER: Neutron Damage Calculations for Materials Irradiations, ANL/FPP/TM-197, January 1985.

[40] S.A. Fetter, E.T. Cheng, F.M. Mann, Fusion Eng. Des. 13 (Nov.) (1990) 239.

[41] S. Reyes, J.F. Latkowski, J. Gomez del Rio, J. Sanz, Fusion Technol. 39 (Mar.) (2001) 941.

[42] S.J. Zinkle, J.P. Robertson, R.L. Klueh, Thermophysical and mechanical properties of Fe-(8–9%)Cr reduced activation steels, in Fusion Materials Semiann. Prog. Report for period ending June 30 1998, DOE/ER-0313/24, Oak Ridge National Lab, 1998, p. 135.

[43] S.J. Zinkle, F.W. Wiffen, Radiation effects in refractory alloys, in: M.S. El-Genk (Ed.), Space Technology and Applications International Forum-STAIF 2004, AIP Conf. Proc., vol. 699, American Institute of Physics, Melville, NY, 2004, p. 733.

[44] S.J. Zinkle, N.M. Ghoniem, Fusion Eng. Des. 51–52 (2000) 55.